Check for updates

Cyclic Compressive Behavior of Hybrid FRP-Confined Concrete

Medine Ispir[1]; Korhan Deniz Dalgic[2]; and Alper Ilki, Aff.M.ASCE[3]

Abstract: The aim of this study is to define the cyclic axial behavior of hybrid FRP (fiber reinforced polymer)-confined concrete based on the results of an experimental study presented here. Two different types of fiber sheets with different ultimate tensile strain capacities were used together in a suitable epoxy resin matrix to confine concrete. The inner and outer jackets of the concrete confinement were constituted with carbon (or glass) sheets with a relatively low tensile strain capacity and polyethylene terephthalate (PET) sheets with a high tensile strain capacity. PET fibers, which are a relatively new type of fiber, are made from recycled plastics. By varying the number of layers of the outer fiber sheet, different combinations were formed for the hybrid jackets. To characterize the cyclic axial behavior of hybrid FRP-confined concrete, experimental data were utilized to obtain the axial stress–strain relationship and dilation behavior. Based on the results, a stress–strain model for the envelope curve of the cyclic response of hybrid FRP-confined concrete is proposed.
DOI: 10.1061/(ASCE)CC.1943-5614.0001156. *© 2021 American Society of Civil Engineers.*

Author keywords: CFRP; Concrete confinement; Compression; Cyclic axial loading; Hybrid confinement; PET-FRP; Large rupture strain.

Introduction

A major application of fiber-reinforced polymers (FRPs) in civil engineering is the external confinement of concrete to increase axial strength and ductility. The experimental research in this field is mostly related to the compression behavior of the specimens under monotonic loads (Ilki and Kumbasar 2003; Teng and Lam 2004; Rousakis and Karabinis 2008; Djafar-Henni and Kassoul 2018; Zeng et al. 2020; Lin et al. 2020; Saleem et al. 2021). However, testing specimens under cyclic loads can provide more evidence to better understand the compression response and to evaluate its ductility during an event having loading and unloading phases, such as earthquakes. The number of studies focusing on the FRP confinement of concrete members under cyclic axial loads is relatively low (Lam et al. 2006; Ilki et al. 2008; Lam and Teng 2009; Bai et al. 2014; Demir et al. 2015; Li and Wu 2015; Yu et al. 2015; Cao et al. 2021).

Recent studies have shown that the use of FRP composites with a large rupture strain (LRS) capacity [i.e., polyethylene terephthalate (PET) and polyethylene naphthalate (PEN)] can strongly improve the ductility of concrete compression members when they are externally wrapped (Dai et al. 2012; Bai et al. 2014; Ispir 2015; Saleem et al. 2017; Han et al. 2020). However, the modulus of elasticity of these materials is low (10–40 GPa). This property means that LRS FRP composites will generate relatively less stress than conventional high modulus FRP composites (i.e., carbon, glass, and aramid fibers) for a certain concrete deformation state. This effect might represent a significant drawback for the prevention of brittle concrete column damage, such as shear damage, which is usually initiated at relatively low strain levels (Anggawidjaja et al. 2006; Zhang et al. 2017; Dai et al. 2012). At these levels, the LRS FRP composite jacket will exert a limited amount of confinement stress and shear contribution to surpass the failure due to its low modulus. This can be overcome by either increasing the thickness of the LRS FRP composite jacket, which can result in other issues, such as being infeasible, or hybridizing LRS fibers with high modulus carbon, glass, or aramid fibers.

PET fibers are obtained by recycling waste plastic bottles and are notably cost-effective compared to high modulus fibers (Ye et al. 2021). By hybridizing PET fibers with high modulus fibers, it is possible to develop environmentally friendly, ductile, and affordable column jacketing configurations. Furthermore, by adjusting the amount of PET fibers in the hybrid jacket, the design of the retrofitting scheme can be tailored according to the specific demands (Ispir et al. 2018).

The number of existing studies on the use of PET fibers in a hybrid scheme is quite limited. Guo et al. (2020), Yu et al. (2017), and Zeng et al. (2020) used PET-FRP composites along with steel tubes to confine concrete specimens under axial compression stresses. Huang et al. (2018) used PET-FRP composites to confine concrete-encased steel columns. In these studies, it was reported that the buckling of steel tubes and encased steel sections was significantly delayed or totally prevented by means of outer PET-FRP composite jackets. This effect led to an increase in axial load capacity and ductility. Nain et al. (2020) developed composite tubes using short (glass) and LRS (PET or PEN) FRP composites to confine high-strength concrete specimens. These researchers observed that specimens confined with hybrid FRP jackets showed better strength enhancement than the specimens confined with only short or only LRS FRP composite jackets.

Most of the current studies aim to develop novel compression members using the hybridization of different FRP composites. However, there is also a strong need for further research on hybrid concrete jacketing solutions to reinforce the substandard existing structures.

[1]Associate Professor, Faculty of Civil Engineering, Istanbul Technical Univ., Maslak, Istanbul 34469, Turkey (corresponding author). ORCID: https://orcid.org/0000-0001-5400-5526. Email: ispirm@itu.edu.tr

[2]Assistant Professor, Dept. of Civil Engineering, Izmir Institute of Technology, Urla, Izmir 35430, Turkey. Email: korhandenizdalgic@iyte.edu.tr

[3]Professor, Faculty of Civil Engineering, Istanbul Technical Univ., Maslak, Istanbul 34469, Turkey. ORCID: https://orcid.org/0000-0002-4853-7910. Email: ailki@itu.edu.tr

Note. This manuscript was submitted on October 7, 2020; approved on June 29, 2021; published online on August 11, 2021. Discussion period open until January 11, 2022; separate discussions must be submitted for individual papers. This paper is part of the ***Journal of Composites for Construction***, © ASCE, ISSN 1090-0268.

Downloaded from ascelibrary.org by IZMIR YUKSEK TEKNOLOJI ENSTITUSU on 05/23/22. Copyright ASCE. For personal use only; all rights reserved.

Understanding and modeling the behavior of low-strength concrete confined with hybrid FRP composite jackets can provide an important basis to develop more efficient and more affordable strengthening strategies for existing substandard reinforced concrete columns.

This study aims to fill this gap in the literature and owes its originality to the cyclic axial testing of relatively low strength (approximately 20 MPa) concrete specimens as being representative of the actual concrete quality used in the existing substandard reinforced concrete buildings. Standard cylinder specimens are jacketed using either only high modulus FRP composites (i.e., carbon and glass FRP composites) or hybrid sheets constructed by combining high modulus and LRS PET-FRP composites. The experimental compressive behaviors of the specimens are comprehensively examined thereafter, and based on the test results of hybrid FRP-confined specimens, a modified stress–strain model is developed.

Experimental Program

Materials and Confinement Configurations

In this study, with the intention of examining the cyclic axial behavior of hybrid-FRP confined concrete, 16 standard cylinder specimens were tested. The specimens had a diameter of 150 mm and a height of 300 mm. The specimens were produced with a ready mixed concrete. The experimental program is presented in Table 1. While 12 specimens were confined with FRP sheets, four specimens were reserved to determine the unconfined compressive strength of concrete. The average unconfined compressive strength (f_{co}) of the concrete at 28 days was determined to be 17.9 MPa by testing two specimens as per TS EN 12390-3 (TSE 2003). The standard deviation was calculated as 1.75 MPa. Unidirectional carbon, glass, and PET sheets were used to confine the specimens. Table 2 shows the characteristics of the fiber sheets, which were provided by the manufacturers. These properties are the typical values obtained from unimpregnated fabric tensile tests. The online data sheets can be found in Yönlü and Kumaş n.d. for carbon and glass and in Maeda Kosen (2002) for PET fiber sheets. While the tensile load-elongation behavior of carbon and glass sheets is linear, that of PET sheets is nonlinear, as represented by Bai et al. (2014), as a cubic polynomial with a descending slope.

Eight specimens were confined with two different FRP types to form inner and outer jackets of hybrid confinement configurations. The remaining four specimens were confined with only one type of FRP sheet. The prominent aspect of the hybrid confinement adopted is the substantial difference in the tensile strain capacities of the fiber sheets used: while PET has an LRS capacity, carbon and glass sheets have a remarkably lower rupture strain capacity (Table 2).

To provide efficient hybridization, while carbon FRP (CFRP) or glass FRP (GFRP) sheets with lower rupture strain and high elastic modulus were used as inner FRP jackets, PET-FRP sheets with a higher deformation capacity were used as outer jackets. To maintain the deformation measurement function of the strain gauges, which were positioned onto the outer jacket, throughout the test, the fiber sheet with lower rupture strain was used as the inner jacket. Each specimen was denoted with a label of $N_1F_1N_2F_2$-C-a/b, where N_1 and N_2 are the number of plies of the inner and outer jackets; F_1 and F_2 are the fiber types of the inner and outer jackets (C: carbon, G: glass, and P: PET); C is the cyclic loading; and a or b is used to differentiate two identical specimens (Table 1). For example, 1C3P-C-b is the second of the identical specimens confined with one layer of CFRP (inner jacket) and 3 layers of PET-FRP (outer jacket) and tested under cyclic compression loading. The specimens confined with a single type of FRP jacket were denoted with NF-C-a/b, where N and F are the number of layers and type of FRP jacket, respectively; C is the cyclic loading; and a or b is used to differentiate two identical specimens. For example, 1G-C-a is the first specimen of two identical specimens confined with one layer of GFRP, which was tested under cyclic loading. The tests for the specimens confined with only PET-FRP were not performed in the current study, since they were tested by Ispir (2015) for another project. It should be noted that the same material and dimensional properties as the specimens presented in this study have been used in that project.

Table 1. Test program

Hybrid FRP-confined specimen	Specimen confined with a single type of FRP jacket
1C1P-C-a	1C-C-a
1C1P-C-b	1C-C-b
1C2P-C-a	
1C2P-C-b	
1C3P-C-a	
1C3P-C-b	
1G1P-C-a	1G-C-a
1G1P-C-b	1G-C-b

Table 2. General characteristics of fiber sheets provided by the manufacturer

Fiber type	Tensile strength f_f (MPa)	Modulus of elasticity E_f (GPa)	Ultimate tensile strain ε_f (%)	Effective thickness t_f (mm)
Carbon	4,900	230	2.1	0.166
Glass	1,700	80	2.8	0.230
PET	740	10	10	1.262

External Jacketing of Specimens

For jacketing of the concrete specimens, a wet lay-up process, which included the following steps, was implemented. As the first step, a primer with two components was applied to each specimen after the surface of the specimen was cleaned. Next, the specimen was left for 6 h to complete curing of the primer. As the second step, a layer of epoxy resin was applied to the surface of the specimen, and the continuous inner fiber sheet impregnated with epoxy resin was subsequently bonded to the concrete surface. The fibers were oriented in the hoop direction. As the last step, another layer of epoxy resin was applied over the wrapped inner fiber sheet, and the outer fibers were bonded. A roller was used to improve resin impregnation between fibers by removing the trapped air. To prevent bond problems between the FRP layers, overlap lengths of 150 mm (CFRP and GFRP) and 150–180 mm (PET-FRP) were formed at the end of the wrapping [Fig. 1(a)]. After the jacketing of the concrete specimens, the upper and lower ends of all specimens were capped with a high-strength mortar to provide uniform distribution of the applied loads.

Test Procedure and Instrumentation

A closed-loop testing machine with a 5,000-kN capacity was used for loading. The tests were run in displacement control with a constant rate of 0.6 mm/min (0.2% vertical strain/min), which included a specified series of unloading–reloading cycles of compression.

Downloaded from ascelibrary.org by IZMIR YUKSEK TEKNOLOJI ENSTITUSU on 05/23/22. Copyright ASCE. For personal use only; all rights reserved.

Each specimen was first loaded to a target level of vertical strain, completely unloaded thereafter, and then reloaded to the next target strain level until the specimen failed. Only one unloading–reloading cycle at each target level was employed. The initial target strain was chosen as 0.5%, and these target strains were applied in increments of 0.5% between 0.5% and 3% and then incremented by 1% until the specimen failed. These strains, which were measured by a built-in LVDT of the test machine, are the ratio of the change in the height of the specimen to the initial height and were automatically applied by the program of the testing machine. The measurement system included two linear variable displacement transducers (LVDTs) with 25-mm capacity and two strain gauges with 60-mm gauge length [Fig. 1(b)]. The LVDTs were used to measure the axial deformations in the center of the specimen throughout a 150-mm gauge length. Strain gauges were used to measure the lateral strain, which was positioned horizontally at the center of the specimens and outside the overlap region. The variation in the FRP jacket lateral strains along the perimeter of the cylinder specimens was studied by Lam et al. (2006). These researchers showed that the measurements of the strain gauges outside the overlapping region differed in an acceptable range and suggested using the average of measured lateral strains read from these strain gauges. The applied loads were measured simultaneously by the built-in load cell of the testing machine. The measurements of loads, vertical deformations, and lateral strains were collected by a data logger and stored in a computer.

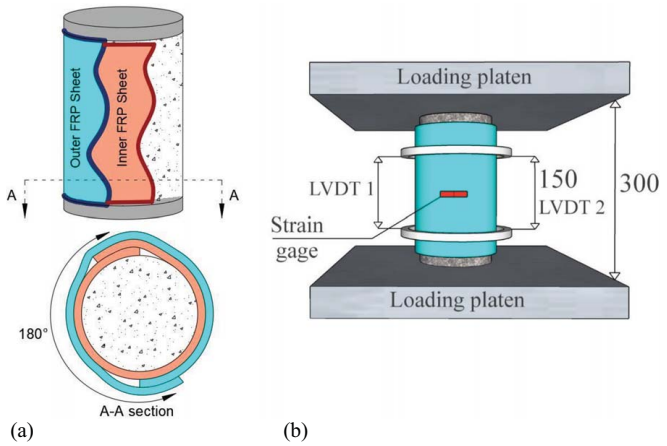

Fig. 1. (a) Hybrid confinement structure; and (b) the measurement system (dimensions in mm).

Test Results

Relationships of Axial Stress–Axial Strain and Axial Stress–Lateral Strain

Conventional FRP-Confined Concrete Specimens

The behavior of the conventional FRP-confined concrete specimens (concrete specimens confined with a single type of high modulus FRP jacket) under cyclic compression loads is presented in Fig. 2. The cyclic axial stress–axial strain and cyclic axial stress–lateral strain curves of 1C (one ply of carbon fiber sheet) and 1G (one ply of glass fiber sheet) specimens are shown in Figs. 2(a and b), respectively. These specimens failed in a brittle manner and loudly due to the sudden rupture of FRP sheets. The lateral strain was calculated as the average of two strain gauges at midheight. It was observed that the measurements of these strain gauges were notably close to each other for the conventional and hybrid FRP-confined concrete tests. This finding may be explained by the explanation given by Li et al. (2016) and Fallah Pour et al. (2020): the use of low strength concrete, stiff FRP jackets, and cyclic loading schemes usually dictates a more homogeneous concrete deformation accumulated at the midheight of the specimens.

As shown in Fig. 2, the specimens confined with a single type of FRP sheet showed an enhanced strength and deformability. The average unconfined compressive strength (f_{co}) was obtained as 24.1 MPa by testing two unconfined specimens at the test period of the confined specimens for at least 150 days. Table 3 presents the strength, deformability, and increase rate ($f_{c,s}/f_{co}$ and $\varepsilon_{c,s}/\varepsilon_{co}$) for the 1C and 1G specimens. In this table, f_{co} is the unconfined concrete strength, $f_{c,s}$ is the FRP-confined concrete strength, ε_{co} is the axial strain at peak stress for unconfined concrete, $\varepsilon_{c,s}$ is the axial strain at peak stress for confined concrete and $\varepsilon_{\text{rup},s}$ is the FRP sheet rupture strain. It should be noted that the subscript s is particularly used in the symbols for presenting the results of the conventional high modulus FRP-confined concrete specimens. The average $f_{c,s}/f_{co}$ ratio and $\varepsilon_{c,s}/\varepsilon_{co}$ ratio are calculated as 2.3 and 14.2 for 1C and 1.8 and 14.0 for 1G specimens, respectively. The average rupture strains ($\varepsilon_{\text{rup},s}$) are calculated as 0.141 for 1C and

Table 3. Test results of a single type of FRP-confined specimen

Specimen	$f_{c,s}$ (MPa)	$f_{c,s}/f_{co}$	$\varepsilon_{c,s}$	$\varepsilon_{c,s}/\varepsilon_{co}$	$\varepsilon_{\text{rup},s}$	$k_{\varepsilon,s}$
1C-a	54.7	2.3	0.0304	14.2	0.0146	0.67
1C-b	55.3	—	0.0261	—	0.0136	—
1G-a	41.0	1.8	0.0290	14.0	0.0195	0.69
1G-b	43.3	—	0.0269	—	0.0192	—

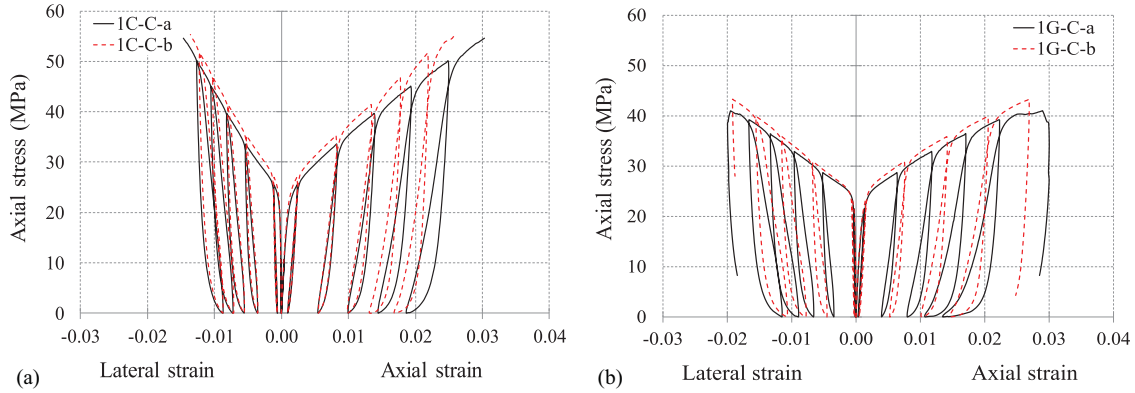

Fig. 2. Cyclic axial stress–axial strain and axial stress–lateral strain relationships for (a) 1C; and (b) 1G specimens.

J. Compos. Constr., 2021, 25(5): 04021045

Downloaded from ascelibrary.org by IZMIR YUKSEK TEKNOLOJI ENSTITUSU on 05/23/22. Copyright ASCE. For personal use only; all rights reserved.

0.194 for 1G. The companion specimens of 1C and 1G tested under monotonic loads by Ispir et al. (2018) displayed similar stress and strain enhancement ratios.

The comparison between FRP sheet ultimate tensile strain capacities (ε_f) that are reported by the supplier (Table 2) and the rupture strains ($\varepsilon_{rup,s}$) measured experimentally (Table 3) shows that the experimental values are lower than the reported tensile strain capacities: rupture strain efficiency factors ($k_{\varepsilon,s}$), which is the ratio of $\varepsilon_{rup,s}/\varepsilon_f$ is lower than 1. The average $k_{\varepsilon,s}$ for the 1C and 1G specimens was found to be 0.67 and 0.69, respectively. The average $k_{\varepsilon,s}$ values for CFRP- and GFRP-confined concrete cylinders were reported to be 0.586 and 0.624 by Lam and Teng (2003), 0.581 and 0.669 by Lam and Teng (2004), and 0.63 and 0.68 by Realfonzo and Napoli (2011), respectively.

The probable causes of lower $\varepsilon_{rup,s}$ values with respect to ε_f were previously explained by underlining two issues: strain localization and in situ properties of the FRP jacket (Pessiki et al. 2001; De Lorenzis and Tepfers 2003). The first is related to the nonuniform strain distribution in the FRP jacket due to mainly nonhomogeneous deformations in the cracked concrete and possible eccentricities of loading. The latter is possible because of local misalignment or waviness of fibers in the wet lay-up process (unequal stretching of the fibers), residual strains due to creep, shrinkage, and temperature effects, and the cumulative possibility of imperfections in the FRP jacket, which is considerably larger in size than a tensile test coupon used for determining the ultimate tensile strain capacity ε_f. Matthys et al. (2006) also pointed out that the multiaxial stress state due to stress transfer between the concrete core and FRP jacket and workmanship might be critical to the reduced efficiency of FRP layers.

Hybrid FRP-Confined Concrete Specimens

The hybrid FRP-confined specimens were tested under cyclic compression loads. The responses of these specimens are given with the cyclic axial stress–axial strain and cyclic axial stress–lateral strain relationships in Figs. 3 and 4.

To simplify the explanation of the stress–strain behavior of hybrid FRP-confined specimens, a schematic envelope curve of the stress–strain relationship is presented in Fig. 5. The envelope curve of each specimen was obtained by connecting the unloading points on the cyclic stress–strain curve. In Fig. 5, the three points characterizing the behavior of the hybrid FRP-confined specimens are indicated with Point 1, Point 2, and Point 3. The axial stress and corresponding axial and lateral strains at these points are symbolized with $f_{c,hn}$, $\varepsilon_{c,hn}$, and $\varepsilon_{l,hn}$, respectively, where the subscript n indicates the point number (Fig. 5). It should be noted that the subscript h is particularly used for presenting the results of the hybrid FRP-confined specimens.

Cyclic compression tests of the hybrid FRP-confined specimens reveal two different types of behavior. Up to Point 1, the shape of the stress–strain curve of the hybrid FRP-confined specimens is very similar to that of the conventional FRP-confined concrete specimens. In this stage, the stress–strain behavior is characterized by two ascending regions.

At Point 1, the inner FRP sheet ruptures at first (the first rupture point, Fig. 5) since the ultimate lateral strain capacity of the inner FRP sheet (CFRP or GFRP) is lower than that of the outer FRP

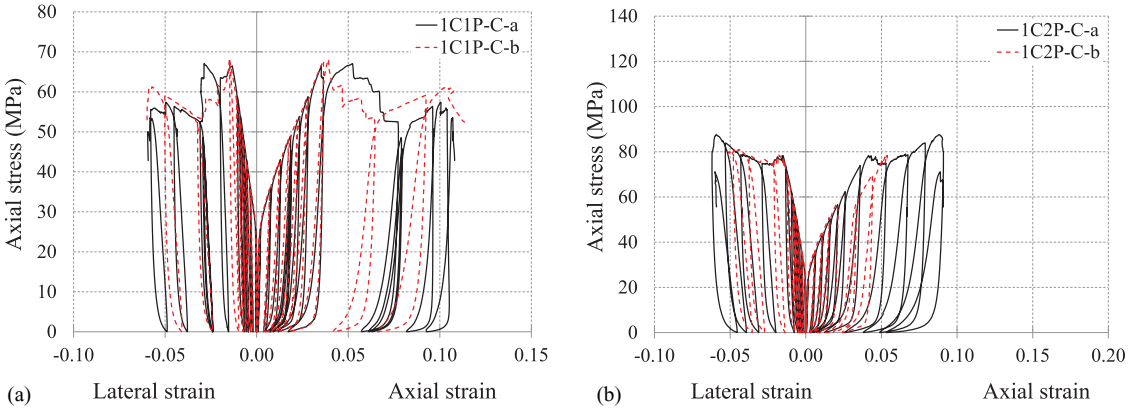

Fig. 3. Cyclic axial stress–axial strain and axial stress–lateral strain relationships of the (a) 1C1P; and (b) 1C2P specimens.

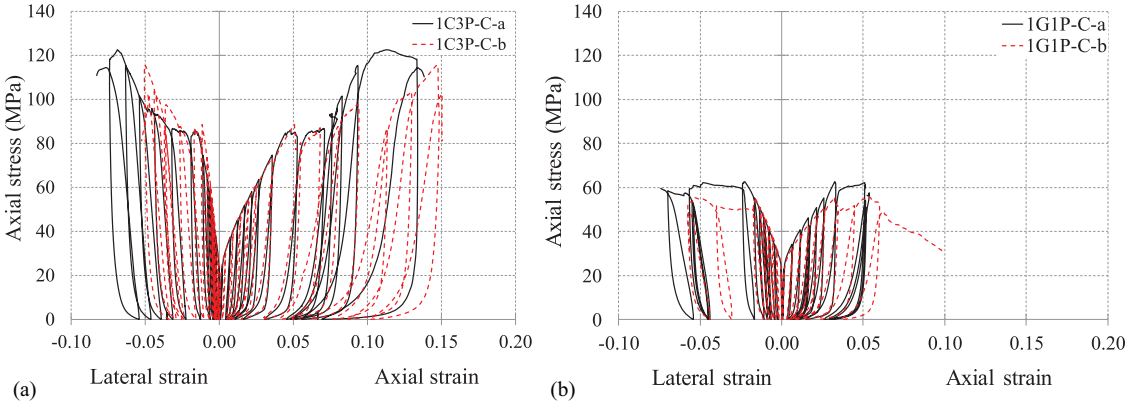

Fig. 4. Cyclic axial stress–axial strain and axial stress–lateral strain relationships of (a) 1C3P; and (b) 1G1P specimens.

J. Compos. Constr., 2021, 25(5): 04021045

Downloaded from ascelibrary.org by IZMIR YUKSEK TEKNOLOJI ENSTITUSU on 05/23/22. Copyright ASCE. For personal use only; all rights reserved.

(PET-FRP). After Point 1, as the inner FRP sheet loses its effectiveness, the hybrid specimen transforms to a specimen confined with only outer FRP sheets (e.g., behaves like 3P in the case of the 1C3P specimen). If the strain and confinement stress capacities in the hoop direction of the outer FRP confinement are greater (or equal to) than the hoop strain and confinement stress at Point 1, the outer FRP elongates from Point 1 to Point 2. If not, the outer FRP sheet will rupture at Point 1 or at a point between Point 1 and Point 2. In this study, this is called the first type of behavior.

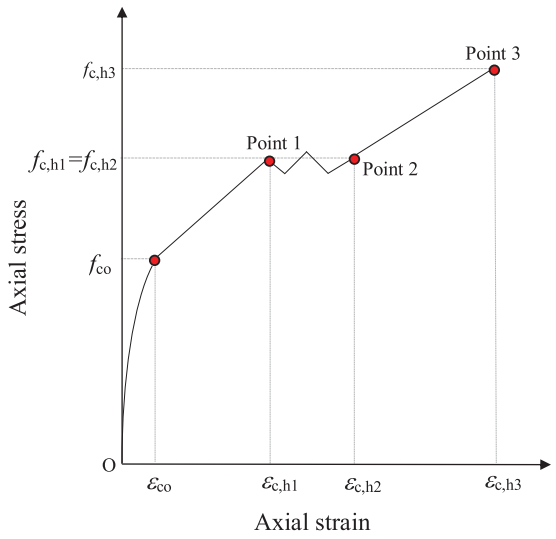

Fig. 5. Representation of the axial stress–axial strain curve for hybrid FRP-confined concrete.

During this rebalancing stage, slight load drops take place, while axial and lateral strains increase. Nevertheless, the stress–strain behavior in this range (between Point 1 and Point 2 in Fig. 5) may be represented with a horizontal line.

Even if the inner and outer FRP sheets have very different ultimate strain capacities, if the confinement stress capacity of the outer FRP layer is equal to the confinement stress exerted at Point1, the outer FRP sheet reaches its rupture strain at Point 2. The 1C1P and 1G1P specimens behave in this way and fail at Point 2 due to the rupture of the outer PET-FRP sheet.

If the strain and confinement stress capacities in the hoop direction of the outer FRP confinement are greater than the hoop strain and confinement stress at Point 2, the hybrid specimen (1C2P and 1C3P) reveals the second type of behavior. An ascending stress–strain region between Point 2 and Point 3 is observed, and the outer FRP jacket fails entirely at Point 3. Ispir et al. (2018) observed similar types of behaviors for the hybrid-confined specimens tested monotonically.

The test outputs are presented in Tables 4–6 for Points 1, 2, and 3. Some values of 1C2P-C-b in Tables 4–6 are signed with *na* since LVDTs were not operating until the end of the specimen test. As expected, since the applied confinement stress at Point 1 is higher in the hybrid specimens, the axial stress and strain values for each hybrid specimen at this point are higher than those of corresponding specimens confined with a single type of FRP jacket. The ratios of $\varepsilon_{l,h1}/\varepsilon_{\mathrm{rup},s}$ show that lateral strains measured from the outer PET-FRP jacket's surface at Point 1 ($\varepsilon_{l,h1}$) are almost the same as the lateral strains that are specified as the rupture strain of the corresponding specimens confined with only a single type of FRP jacket ($\varepsilon_{\mathrm{rup},s}$). Based on this outcome, the inner and outer FRP sheets work together as an integrated FRP jacket. The average

Table 4. Test results for hybrid FRP-confined specimens at Point 1

Specimen	$f_{c,h1}$ (MPa)	$f_{c,h1}/f_{co}$	$f_{c,h1}/f_{c,s}$	$\varepsilon_{c,h1}$	$\varepsilon_{c,h1}/\varepsilon_{co}$	$\varepsilon_{c,h1}/\varepsilon_{c,s}$	$\varepsilon_{l,h1}$	$\varepsilon_{l,h1}/\varepsilon_{\mathrm{rup},s}$	$\varepsilon_{l,h1}/\varepsilon_{f}$
1C1P-C-a	66.5	2.8	1.2	0.0353	18.6	1.3	0.0133	1.01	0.68
1C1P-C-b	68.1	—	—	0.0391	—	—	0.0151	—	—
1C2P-C-a	78.3	3.2	1.4	0.0415	23.5	1.7	0.0150	1.06	0.71
1C2P-C-b	77.6	—	—	0.0523	—	—	0.0150	—	—
1C3P-C-a	84.7	3.6	1.6	0.0447	23.9	1.7	0.0143	0.92	0.62
1C3P-C-b	88.6	—	—	0.0507	—	—	0.0116	—	—
1G1P-C-a	62.5	2.5	1.4	0.0323	16.2	1.2	0.0226	1.01	0.70
1G1P-C-b	55.6	—	—	0.0323	—	—	0.0164	—	—

Table 5. Test results for hybrid-confined specimens at Point 2

Specimen	$f_{c,h2}$ (MPa)	$f_{c,h2}/f_{co}$	$f_{c,h2}/f_{c,h1}$	$\varepsilon_{c,2}$	$\varepsilon_{c,h2}/\varepsilon_{co}$	$\varepsilon_{c,h2}/\varepsilon_{c,h1}$	$\varepsilon_{l,h2}$	$k_{\varepsilon,h2}$
1C1P-C-a	55.5	2.4	0.9	0.1040	52.4	2.8	0.0578	0.58
1C1P-C-b	60.9	—	—	0.1056	—	—	0.0583	—
1C2P-C-a	78.3	3.2	1.0	0.0627	31.4	1.3	0.0391	—
1C2P-C-b	77.9	—	—	na	—	—	0.0357	—
1C3P-C-a	86.4	3.6	1.0	0.0710	37.9	1.6	0.0320	—
1C3P-C-b	87.7	—	—	0.0806	—	—	0.0266	—
1G1P-C-a	62.2	2.4	1.0	0.0509	26.3	1.6	0.0484	0.51
1G1P-C-b	55.4	—	—	0.0541	—	—	0.0541	—

Table 6. Test results for hybrid-confined specimens at Point 3

Specimen	$f_{c,h3}$ (MPa)	$f_{c,h3}/f_{co}$	$f_{c,h3}/f_{c,h2}$	$\varepsilon_{c,3}$	$\varepsilon_{c,h3}/\varepsilon_{co}$	$\varepsilon_{c,h3}/\varepsilon_{c,h2}$	$\varepsilon_{l,h3}$	$k_{\varepsilon,h3}$
1C2P-C-a	87.5	3.5	1.1	0.0882	44.1	1.4	0.0591	0.53
1C2P-C-b	81.0	—	—	na	—	—	0.0462	—
1C3P-C-a	122.6	4.9	1.4	0.1129	65.0	1.7	0.0687	0.60
1C3P-C-b	115.4	—	—	0.1471	—	—	0.0503	—

Downloaded from ascelibrary.org by IZMIR YUKSEK TEKNOLOJI ENSTITUSU on 05/23/22. Copyright ASCE. For personal use only; all rights reserved.

efficiency factor at Point 1 (average $\varepsilon_{l,h1}/\varepsilon_f$ ratio in Table 4) is calculated as 0.67 for hybrid FRP-confined specimens with inner CFRP jackets. This ratio was obtained as 0.70 for monotonically tested hybrid FRP-confined specimens with inner CFRP jackets by Ispir et al. (2018). It should be stated that the companion specimens tested under monotonic loads displayed similar stress and strain enhancements.

Tables 5 and 6 show the numerical values obtained or derived for Points 2 and 3. For these points, despite the loss of the inner FRP sheet(s), the axial compressive stresses $f_{c,h2}$ (at Point 2) and $f_{c,h3}$ (at Point 3) are still notably higher than the unconfined concrete strength ($f_{c,h2}/f_{co}$ and $f_{c,h3}/f_{co} > 1$). Note that the 1C1P and 1G1P specimens do not reach Point 3. It may be considered that due to the large deformations, the 1C3P-C-b specimen deviates from the 1C3P-C-a specimen in the final loading stage (Fig. 4).

The variation of the FRP sheet strain efficiency with regard to the loading type (monotonic or cyclic) and hybridization configuration is evaluated using efficiency factors calculated as the average value of $\varepsilon_{l,hn}/\varepsilon_f$ of identical specimens (Table 7). As seen in Table 7, the hybridization generally resulted in a lower efficiency factor for the outer PET-FRP jacket. This is thought to be because of the nonhomogeneity of concrete damages inside which is much more severe at the ultimate cases of the hybrid cases. For the specimens confined with PET-FRP only, the efficiency factor tends to be higher, as the ultimate axial deformation of the concrete and thus the damage severity of the concrete core is generally lower than that of hybrid FRP-confined specimens.

Dilation Behavior

Conventional FRP-Confined Concrete Specimens

The influence of FRP confinement on the deformation characteristics of concrete can be analyzed by examining lateral strain–axial strain relationships. Fig. 6 presents these relationships of the specimens confined with one layer of CFRP or GFRP. The curves of these relationships are in the form of an increasing function including three parts [Figs. 6(a and b)].

The first part [Fig. 6(b)] is governed by the elastic behavior of the unconfined concrete where lateral deformations are not large enough to elicit the effect of FRP confinement. Hence, the lateral strain–axial strain relationships for all of the specimens coincided with each other in this part, since they were produced using the same concrete. The salient property of this part is that concrete displays a linear elastic behavior. The slope of this linear part, which is known as the elastic Poisson's ratio, is calculated as 0.20–0.22 for the specimens tested. At the transition point between the first and second parts, the axial stress level is between 60% and 70% of the unconfined concrete strength, and the average axial strain is approximately 0.07%, where the first microcracks in the concrete are assumed to occur. The second part [Fig. 6(b)] is governed by the increase in concrete expansion with unstable cracks. Hence, the rate of the lateral strain increase in the second part is higher than that in the first part. The third part [Fig. 6(a)] is governed by the properties of the FRP jacket, and the confinement pressure increases in a passive way, which restrains the lateral strains. Therefore, the rate of increase of lateral strain decreases compared to the second part.

Furthermore, compared to the concrete specimens confined with GFRP jackets, those confined with CFRP jackets have less lateral strain for a given axial strain level. This finding is observed because the CFRP jacket has a higher elastic modulus and accordingly a higher confinement pressure. Such a relationship between lateral strain, axial strain, and lateral confinement stress was also determined by Lim and Ozbakkaloglu (2015) and Ribeiro et al. (2018).

Table 7. Comparison of the lateral-strain efficiency factor for different loadings and specimen types

Specimen	Cyclic tests (current tests)	Monotonic tests (Ispir et al. 2018)	Tests of only PET-FRP confined specimens (Ispir 2015)	
			Cyclic	Monotonic
1C1P	0.58	0.70	0.54 (1P)	0.82 (1P)
1G1P	0.51	0.61	0.54 (1P)	0.82 (1P)
1C2P	0.53	0.69	0.84 (2P)	0.77 (2P)
1C3P	0.60	0.64	0.78 (3P)	0.74 (3P)

Hybrid FRP-Confined Specimens

The analysis of Figs. 7(a and b) reveals that the dilation behavior of the hybrid specimens can be characterized in four parts. Similar to conventional FRP-confined cases, the curves of the lateral strain and axial strain relationships are in the form of an increasing function. The first parts are governed by the behavior of the unconfined concrete up to a point corresponding to an axial stress level of 60%–80% of the unconfined concrete strength or to an average axial strain of 0.08% approximately (Fig. 7). In this part, the lateral strain–axial strain behavior of all of the specimens almost coincides with the exception of the 1G1P specimen [Fig. 7(b)]. Poisson's ratio is calculated as 0.17–0.25 based on the slopes of the first parts. In the second part, the relationship exhibits nonlinear behavior up to the unconfined concrete strength [Fig. 7(b)]. Next, in the

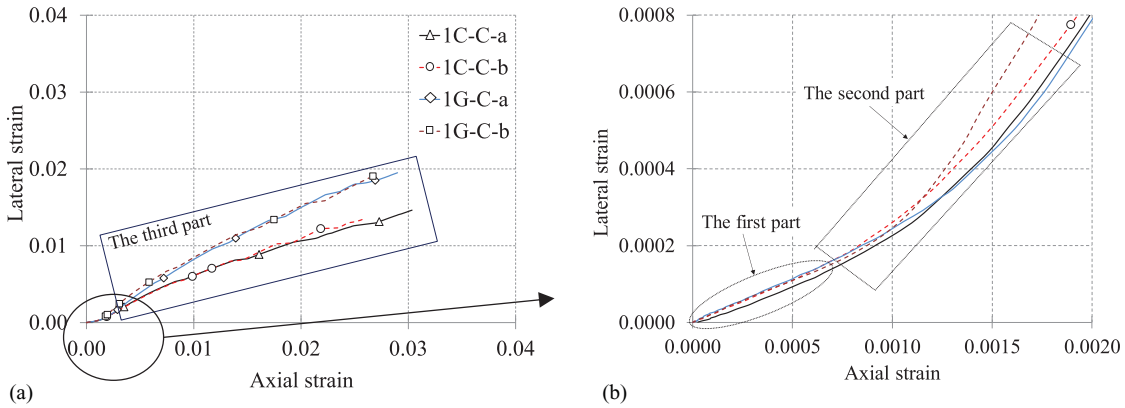

Fig. 6. Lateral strain–axial strain relationships of conventional FRP-confined specimens: (a) normal view; and (b) close-up view for the first and second parts.

J. Compos. Constr., 2021, 25(5): 04021045

Downloaded from ascelibrary.org by IZMIR YUKSEK TEKNOLOJI ENSTITUSU on 05/23/22. Copyright ASCE. For personal use only; all rights reserved.

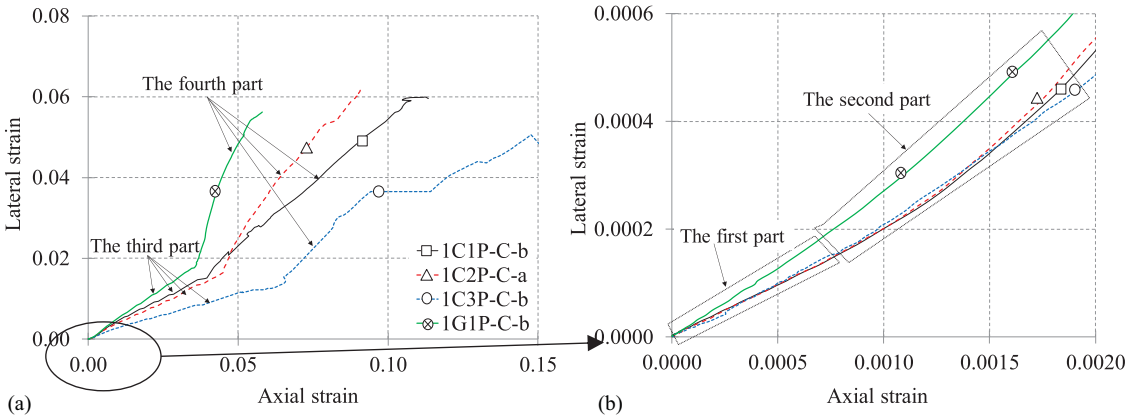

Fig. 7. Lateral strain–axial strain relationships of hybrid FRP-confined specimens: (a) normal view; and (b) close-up view for the first and second parts.

third part, due to the activation of the confinement pressure, the relationship is governed by the properties of the hybrid FRP jacket [Fig. 7(a)]. The rate of increase of lateral strain in this part decreases with respect to the second part because of the confinement of the concrete [Figs. 7(a and b)]. In this part, for a given axial strain level, while 1G1P has the largest lateral strain, 1C3P has the least lateral strain. This finding is observed because the confinement stress applied by 1G1P is remarkably lower than that applied by 1C3P. This part continues until the inner FRP sheet ruptures. Next, the outer FRP jacket governs the last part (the fourth part), and the lateral strains start increasing rapidly up to the failure of the outer PET-FRP jacket. The junction point between the third and last parts [Fig. 7(a)] corresponds to the rupture of the inner FRP sheet (Point 1 in Fig. 5). The slope of the last parts demonstrates that as the confinement pressure provided by the outer FRP jacket increases, the increase rate of the lateral strain decreases.

Modeling the Stress–Strain Relationship for Hybrid FRP-Confined Concrete

To predict the envelope axial stress–axial strain curve of hybrid FRP-confined concrete, a modified model is proposed. The modifications are based on the observed behaviors of the specimens tested in both this study and Ispir et al. (2018). The two main steps of the development of the proposed model are to first plot the basic shape of the stress–strain curve similar to Fig. 5 and then predict the key stresses and strains of each point on the stress–strain curve. These steps are detailed as follows:

Determination of Basic Shape of the Stress–Strain Curve

As the first step of developing the proposed model, the shape of the axial stress–strain curve for hybrid FRP-confined concrete is predicted considering the knowledge on the types of behaviors explained in the "Test Results" section. The algorithm in Fig. 8 is proposed to plot the shape of the axial stress–strain relationship. This algorithm applies to hybridization schemes with at most two different types of constituting FRP sheets. On the other hand, to be able to use this algorithm, the inner jacket should be constructed using an FRP sheet with a lower ultimate tensile strain capacity than the outer jacket. Hence, the inner FRP sheet is expected to rupture first at Point 1 (Fig. 5).

The first two parts of the axial stress–axial strain curve of the hybrid FRP-confined concrete are identical to the case of concrete confined with a single type of FRP. The rest of the curve can be predicted considering the total lateral confinement stress at Point 1 [Eq. (1)], the ultimate tensile strain capacities of the constituent FRP sheets and the ultimate confinement stress that can be applied by the outer FRP sheet [Eq. (2)]. During the implementation of this algorithm, it is considered that the lateral strains of the inner and outer jackets at Point 1 ($\varepsilon_{l,h1}$) are equal, and they take a value of $(k_\varepsilon \times \varepsilon_f)_{\text{inner}}$, where ε_f is the ultimate tensile strain capacity of the inner fiber sheet provided by the manufacturer. For the presented study, $(k_\varepsilon)_{\text{inner}}$ is taken as 0.7. This value is the average of the efficiency factors of CFRP and GFRP, which were obtained from the current tests of the hybrid-confined and conventional confined-concrete specimens. For the calculation of ultimate confinement stress capacity of the outer jacket, $(f_{lu})_{\text{outer}}$, the lateral strain efficiency factor of the outer jacket should be used. For the presented study, $(k_\varepsilon)_{\text{outer}}$ is taken as 0.56 in Eq. (2), which was calculated from the average rupture strain of the hybrid-confined specimens tested in this study.

$$f_{l,h1} = \left(\frac{2E_f \varepsilon_{l,h1} n_f t_f}{D}\right)_{\text{inner}} + \left(\frac{2E_f \varepsilon_{l,h1} n_f t_f}{D}\right)_{\text{outer}} \times (\varepsilon_{l,h1})_{\text{outer}} = (\varepsilon_{l,h1})_{\text{inner}} \tag{1}$$

$$(f_{lu})_{\text{outer}} = \left(\frac{2E_f k_\varepsilon \varepsilon_f n_f t_f}{D}\right)_{\text{outer}} \tag{2}$$

To plot the shape of the stress–strain curve, the lateral strain at Point 2 of the outer FRP jacket should also be calculated. The outer FRP sheet should display an elongation in the hoop direction between Points 1 and 2 to compensate for the total lateral stress that was initially exerted by the inner and outer jackets together at Point 1. During this elongation that takes place to rebalance the lateral confinement stresses at Point 1 and Point 2, slight fluctuations are observed in axial compression stress. Equating the lateral confinement stresses at Point 1 and Point 2, Eq. (3) is derived to calculate the lateral strain at Point 2 ($\varepsilon_{l,h2c}$). $\varepsilon_{l,h1}$ is the lateral strain immediately before rupturing of the inner FRP sheet (at Point 1); $f_{l,h1}$ is the total lateral confinement stress at Point 1, which is calculated by substituting $\varepsilon_{l,h1}$ into Eq. (1); D is the diameter of the concrete specimen without considering the thickness of the FRP jackets, and n_f is the number of FRP layers. The calculated and measured lateral strains at Point 2 ($\varepsilon_{l,h2c}$, $\varepsilon_{l,h2}$) are presented in Table 8 together with $\varepsilon_{l,h1}$ and $f_{l,h1}$.

$$\varepsilon_{l,h2c} = \frac{f_{l,h1} D}{(2E_f n_f t_f)_{\text{outer}}} \tag{3}$$

Downloaded from ascelibrary.org by IZMIR YUKSEK TEKNOLOJI ENSTITUSU on 05/23/22. Copyright ASCE. For personal use only; all rights reserved.

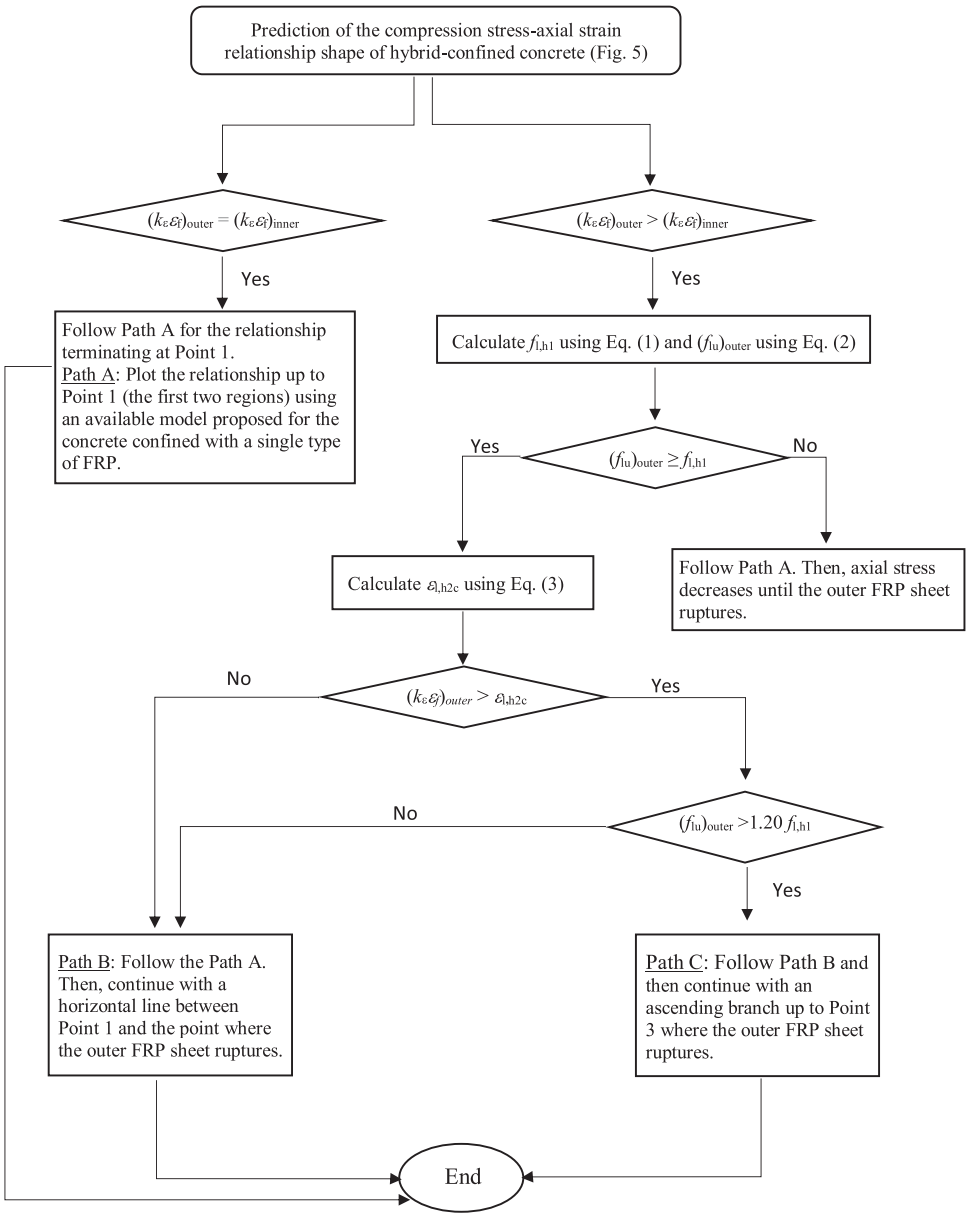

Fig. 8. Flowchart for the basic shape of the axial stress–axial strain relationship.

Table 8. Predicted lateral strains at Point 2 ($\varepsilon_{l,h2c}$)

Specimen	Test $\varepsilon_{l,h1}$	Calculated $f_{l,h1}$ (MPa)	Calculated $\varepsilon_{l,h2c}$	Test $\varepsilon_{l,h2}$	$\varepsilon_{l,h2}$ ratio (test/calculated)
1C1P	0.0147	9.9	0.0609	0.0581	0.95
1C2P	0.0147	12.4	0.0380	0.0374	0.98
1C3P	0.0147	14.9	0.0304	0.0293	0.96
1G1P	0.0196	8.1	0.0471	0.0513	1.09

Table 9. Shape of the stress–strain curves of the hybrid-confined specimens

Specimen	$f_{l,h1}$	$(f_{lu})_{outer}$	Comparison $[(f_{lu})_{outer}/f_{l,h1}]$	Shape
1C1P	9.9	9.4	0.95	Path B
1C2P	12.4	18.8	1.52	Path C
1C3P	14.9	28.2	1.89	Path C
1G1P	8.1	9.4	1.16	Path B

The calculated $\varepsilon_{l,h2c}$ strains are in good agreement with the $\varepsilon_{l,h2}$ strains obtained from the current tests. According to the test results, $(f_{lu})_{outer}/f_{l,h1}$ must be greater than 1.20 for the specimen to exhibit an ascending behavior after Point 2, (Table 9). By applying the algorithm presented in Fig. 8, the stress–strain curve for each hybrid-confined specimen is determined (Fig. 9).

Predictions of the Key Stress and Strain

After the basic shape of the axial stress–axial strain curve is determined, as the second step, the values of the key stresses and strains are predicted. In the following calculations, lateral strains at Point 1 ($\varepsilon_{l,h1}$) and Point 3 ($\varepsilon_{l,h3}$) are taken as the effective lateral strains [$(k_\varepsilon\varepsilon_f)_{inner}$ and $(k_\varepsilon\varepsilon_f)_{outer}$, respectively]. The lateral strain at Point 2 ($\varepsilon_{l,h2c}$) is obtained using Eq. (3).

Up to Point 1, the inner and outer jackets are accepted to be completely integrated. For this part, the model proposed by Lam and Teng (2003) is utilized. This model consists of two regions:

J. Compos. Constr., 2021, 25(5): 04021045

Downloaded from ascelibrary.org by IZMIR YUKSEK TEKNOLOJI ENSTITUSU on 05/23/22. Copyright ASCE. For personal use only; all rights reserved.

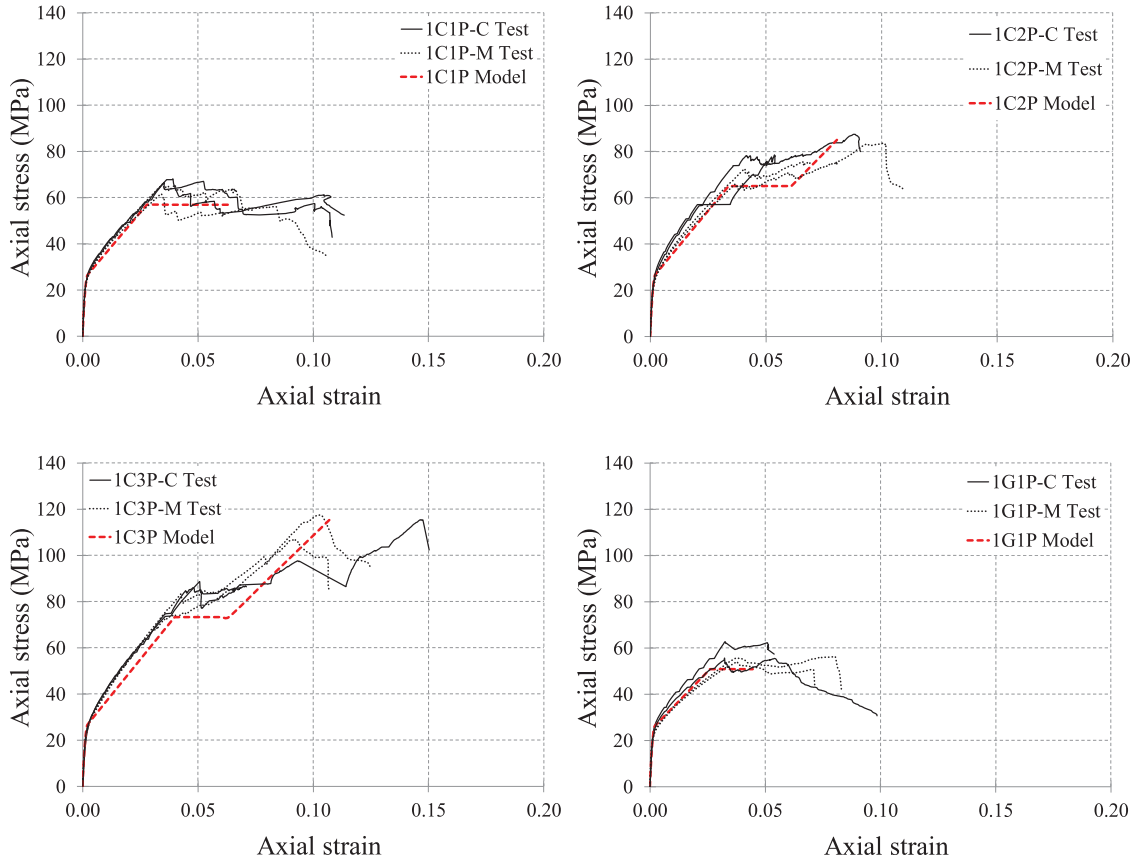

Fig. 9. Comparison of axial stress–axial strain curves obtained from the proposed model and tests.

the first region is defined with a parabolic function [Eq. (4*a*)], and the second region is defined with a linear function [Eq. (4*b*)]. The required expressions of this model are given in Eqs. (4)–(10). In these equations, σ_c is the compression stress, ε_c is axial strain, and E_c is the modulus of concrete [Eq. (5)]. f_o and ε_t are the stress and axial strain, respectively, where the parabolic first portion meets the linear second region. f_o is taken as f_{co} and ε_t is calculated by Eq. (6). E_2 is the slope of the second region of the stress–strain curve [Eq. (7)]. f_{cc} is the compressive strength of confined concrete [Eq. (8)] and ε_{cu} is the ultimate axial strain of confined concrete [Eq. (9)]. f_{lu} is the ultimate confinement stress [Eq. (10)] and $\varepsilon_{h,\text{rup}}$ is the FRP hoop rupture strain in FRP-confined concrete.

$$\sigma_c = E_c\varepsilon_c - \frac{(E_c - E_2)^2}{4f_o}\varepsilon_c^2 \quad 0 \le \varepsilon_c \le \varepsilon_t \tag{4a}$$

$$\sigma_c = f_o + E_2\varepsilon_c \quad \varepsilon_t \le \varepsilon_c \le \varepsilon_{cu} \tag{4b}$$

$$E_c = 4{,}730\sqrt{f_{co}} \tag{5}$$

$$\varepsilon_t = \frac{2f_o}{(E_c - E_2)} \tag{6}$$

$$E_2 = \frac{f_{cc} - f_o}{\varepsilon_{cu}} \tag{7}$$

$$\frac{f_{cc}}{f_{co}} = 1 + 3.3\frac{f_{lu}}{f_{co}} \tag{8}$$

$$\frac{\varepsilon_{cu}}{\varepsilon_{co}} = 1.75 + 12\left(\frac{f_{lu}}{f_{co}}\right)\left(\frac{\varepsilon_{h,\text{rup}}}{\varepsilon_{co}}\right)^{0.45} \tag{9}$$

$$f_{lu} = \frac{2E_f n_f t_f \varepsilon_{h,\text{rup}}}{D} \tag{10}$$

After Point 1, the stress at Point 2 ($f_{c,h2}$) is accepted as equal to the stress at Point 1 ($f_{c,h1}$).

The axial strain at Point 2 ($\varepsilon_{c,h2}$) is considered the summation of the axial strain at Point 1 ($\varepsilon_{c,h1}$) and the axial strain increment $(\Delta\varepsilon_c)_{1\to2}$ between Point 1 and Point 2, which is mathematically expressed in Eq. (11). To estimate $(\Delta\varepsilon_c)_{1\to2}$, Eq. (12) can be used to show that confinement stress (f_{lu}) and lateral rupture strain ($\varepsilon_{h,\text{rup}}$) terms should be replaced by the differential values of those terms between Points 1 and 2. Eq. (12) is the re-expressed form of Eq. (9). Eq. (13) shows the calculation of the differential value of confinement stress between these points ($(\Delta f_l)_{1\to2}$). $\varepsilon_{c,h2}$ is calculated through Eqs. (11)–(13) for each specimen.

$$\varepsilon_{c,h2} = \varepsilon_{c,h1} + (\Delta\varepsilon_c)_{1\to2} \tag{11}$$

$$(\Delta\varepsilon_c)_{1\to2} = 0.002\left[1.75 + 12\left(\frac{(\Delta f_l)_{1\to2}}{f_{co}}\right)\left(\frac{\varepsilon_{l,h2} - \varepsilon_{l,h1}}{\varepsilon_{co}}\right)^{0.45}\right] \tag{12}$$

$$(\Delta f_l)_{1\to2} = \left(\frac{2E_f n t_f}{D}\right)_{\text{outer}}(\varepsilon_{l,h2} - \varepsilon_{l,h1}) \tag{13}$$

The expression of Eq. (8) proposed by Lam and Teng (2003) is used to estimate the axial compression stress at Point 3 ($f_{c,h3}$). As the inner FRP jacket ruptures at Point 1, the confinement stress at Point 3 can be calculated simply by considering that only the outer jacket provides confinement at ultimate. Consequently, the

Downloaded from ascelibrary.org by IZMIR YUKSEK TEKNOLOJI ENSTITUSU on 05/23/22. Copyright ASCE. For personal use only; all rights reserved.

Table 10. Proposed model predictions

Specimen	Point	Test		Predicted		Predicted/test	
		Stress (MPa)	Strain	Stress (MPa)	Strain	Stress ratio	Strain ratio
1C1P	Point 1	65.6	0.0358	57.0	0.0278	0.87	0.78
	Point 2	59.0	0.0899	57.0	0.0631	0.97	0.70
1C2P	Point 1	73.6	0.0437	65.1	0.0339	0.89	0.78
	Point 2	74.3	0.0618	65.1	0.0610	0.88	0.99
	Point 3	83.5	0.0943	86.1	0.0807	1.03	0.86
1C3P	Point 1	82.7	0.0444	73.3	0.0399	0.89	0.90
	Point 2	83.2	0.0638	73.3	0.0634	0.88	0.99
	Point 3	115.7	0.1136	117.8	0.1074	1.01	0.95
1G1P	Point 1	57.0	0.0350	50.9	0.0260	0.89	0.74
	Point 2	56.0	0.0622	50.9	0.0445	0.91	0.72

ultimate confinement stress is calculated with Eq. (2) to determine $f_{c,h3}$. As the 1C2P and 1C3P specimens failed at Point 3, the calculation of $f_{c,h3}$ is necessary for these specimens.

The axial strain at Point 3 ($\varepsilon_{c,h3}$) is calculated with Eq. (14) by following the same approach explained for $\varepsilon_{c,h2}$ above. To estimate the axial strain increment between Points 2 and 3 ($(\Delta\varepsilon_c)_{2\to3}$), Eqs. (15) and (16) are set by replacing the lateral strain in Eqs. (9) and (10) with the differential values of lateral strain between Point 3 and Point 2. Using Eqs. (14) and (16), $\varepsilon_{c,h3}$ is calculated for the 1C2P and 1C3P specimens.

$$\varepsilon_{c,h3} = \varepsilon_{c,h2} + (\Delta\varepsilon_c)_{2\to3} \tag{14}$$

$$(\Delta\varepsilon_c)_{2\to3} = 0.002\left[1.75 + 12\left(\frac{(\Delta f_l)_{2\to3}}{f_{co}}\right)\left(\frac{\varepsilon_{l,h3} - \varepsilon_{l,h2}}{\varepsilon_{co}}\right)^{0.45}\right] \tag{15}$$

$$(\Delta f_l)_{2\to3} = \left(\frac{2E_f n t_f}{D}\right)_{\text{outer}} (\varepsilon_{l,h3} - \varepsilon_{l,h2}) \tag{16}$$

Following these steps, the key values of each point on the stress–strain curve are calculated for each hybrid-confinement configuration. By placing these values on the predicted stress–strain shape, the entire stress–strain path is obtained. The predicted and experimental curves are presented in Fig. 9. In addition to the current experimental curves, those of the monotonic tests given in Ispir et al. (2018) are also provided in Fig. 9. The performance of the proposed model is evaluated over the results obtained from both the cyclic and monotonic tests. These figures show the existence of a reasonable agreement between the experimental and predicted curves. A general underestimation for all of the key stress and strains is because of the underestimation of stress and strain values at Point 1 by Lam and Teng (2003) model. Since the expressions of the modified model are interdependent, underestimation of the stress and strain values of Point 1 results in the underestimation of the following stress and strain values.

The stress and strain values at Points 1–3 predicted with the proposed model are given in Table 10 together with the corresponding test results on average obtained from both cyclic and monotonic tests. To evaluate the performance of the modified model, the statistical parameters of the average absolute error (AAE), mean (M), and standard deviation (SD) of the predictions are calculated using Eqs. (17)–(19). The mean is used to identify the estimation level of the model on average (i.e., overestimation or underestimation) with respect to the corresponding test results. In these equations, m_i and t_i are the value predicted by the model and the corresponding value determined by the test, respectively, and n is the number of tested specimens.

$$\text{AAE} = \frac{\sum_{i=1}^{n} |(m_i - t_i)/t_i|}{n} \tag{17}$$

$$M = \frac{\sum_{i=1}^{n} m_i/t_i}{n} \tag{18}$$

$$\text{SD} = \sqrt{\frac{\sum_{i=1}^{n} ((m_i/t_i) - M)^2}{n-1}} \tag{19}$$

By evaluating the key stress (strain) predictions at Points 1–3 together, the AAE and M values are calculated as 0.09 (0.16) and 0.92 (0.84) with an SD of 0.06 (0.11). Wu and Zhou (2010) defined the accuracy of a model depending on AAE: Category I (AAE $\leq$ 15%—high accuracy), Category II (15% < AAE $\leq$ 30%—moderate accuracy), or Category III (AAE > 30%—low accuracy). Accordingly, the modified model can be classified as Category I in terms of stress and as Category II in terms of strain. An overall assessment of the stress–strain curves and the statistical parameters shows that the modified model can be used to predict the stress–strain curves of hybrid FRP-confined concrete specimens.

Conclusions

The cyclic axial responses of hybrid FRP-confined concrete cylinders were examined experimentally. Hybridization was formed by the use of different types of FRP sheets with different ultimate lateral strain capacities as inner and outer jackets. The assessment of the results of the test and analytical studies leads to the following conclusions:

1. The hybrid-confined specimens tested under axial compression loads exhibited two different types of behaviors depending on the lateral confinement stress and tensile strain capacities of the outer FRP jacket. While the use of PET-FRP as an outer jacket fulfilled a high elongation capacity demand, which is required for efficient hybridization, its lateral confinement stress capacity was decisive for the formation of these behaviors.
2. Although the lateral strain efficiencies of the entire hybrid configurations considered are consistently better under monotonic loadings, no clear sign of superior compression response was observed compared to the cyclically tested specimens.
3. The general rules of FRP-confined concrete, such as greater confinement stress and less concrete core dilatation, apply to the present hybrid case.

J. Compos. Constr., 2021, 25(5): 04021045

Downloaded from ascelibrary.org by IZMIR YUKSEK TEKNOLOJI ENSTITUSU on 05/23/22. Copyright ASCE. For personal use only; all rights reserved.

4. Based on the revealed behaviors of hybrid FRP-confined concrete, a stress–strain model was proposed. Good agreement was observed between the predicted and experimental stress–strain curves.

Data Availability Statement

All data, models, and codes generated or used during the study appear in the published article.

Acknowledgments

The authors are grateful to Maeda Kosen Co. Ltd., Fukui, Japan and Mr. Nakai Hiroshi for providing PET sheets, to BASF Company for providing carbon/glass sheets and epoxy, and to ISTON AS company for providing ready mixed concrete. The authors are also thankful to Amin Nasrinpour, Saeid Hajihosseynlou, and Gorkem Dalgic for their assistance during the tests.

Notation

The following symbols are used in this paper:

D = diameter of the concrete specimen without considering the thickness of the FRP jackets;
E_c = modulus of elasticity of concrete;
$f_{c,h2}$ = axial compressive stress at Point 2;
$f_{c,h3}$ = axial compressive stress at Point 3;
$f_{c,hn}$ = axial compression stress at Point n on the stress–strain relationship of hybrid FRP confined concrete;
$f_{c,s}$ = FRP-confined concrete strength;
f_{cc} = compressive strength of confined concrete;
f_{co} = average unconfined compressive strength;
$f_{l,h1}$ = total lateral confinement stress at Point 1;
f_{lu} = ultimate confinement stress;
$(f_{lu})_{\text{outer}}$ = ultimate confinement stress capacity of the outer jacket;
f_o = stress where the parabolic first portion meets the linear second region;
$k_{\varepsilon,s}$ = rupture strain efficiency factors;
M = mean;
n = number of tested specimens;
n_f = number of FRP layers;
$((\Delta f_l)_{1\to 2})$ = differential value of confinement stress between Points 1 and 2;
$(\Delta\varepsilon_c)_{1\to 2}$ = axial strain increment between Point 1 and Point 2;
$\varepsilon_{c,h2}$ = axial strain at Point 2;
$\varepsilon_{c,hn}$ = axial strain at Point n on the stress–strain relationship of hybrid FRP-confined concrete;
$\varepsilon_{c,s}$ = axial strain at peak stress for confined concrete;
ε_c = axial strain;
ε_{co} = axial strain at peak stress for unconfined concrete;
ε_{cu} = ultimate axial strain of confined concrete;
ε_f = ultimate tensile strain capacity of FRP sheet;
$\varepsilon_{h,\text{rup}}$ = FRP hoop rupture strain in FRP-confined concrete;
$\varepsilon_{l,h1}$ = lateral strains measured from the outer PET-FRP jacket surface at Point 1;
$\varepsilon_{l,h2}$ = lateral strains measured from the outer PET-FRP jacket surface at Point 2;
$\varepsilon_{l,h2c}$ = lateral strains calculated using Eq. (3);
$\varepsilon_{l,h3}$ = lateral strains measured from the outer PET-FRP jacket surface at Point 3;
$\varepsilon_{l,hn}$ = lateral strains measured from the outer PET-FRP jacket surface at Point n corresponding to a specific point on the stress–strain relationship of hybrid FRP confined concrete;
$\varepsilon_{\text{rup},s}$ = FRP sheet rupture strain of the specimen confined with a single type of FRP;
ε_t = axial strain where the parabolic first portion meets the linear second region; and
σ_c = compressive stress.

References

Anggawidjaja, D., T. Ueda, J. Dai, and H. Nakai. 2006. "Deformation capacity of RC piers wrapped by new fiber-reinforced polymer with large fracture strain." *Cem. Concr. Compos.* 28 (10): 914–927. https://doi.org/10.1016/j.cemconcomp.2006.07.011.

Bai, Y.-L., J.-G. Dai, and J. G. Teng. 2014. "Cyclic compressive behavior of concrete confined with large rupture strain FRP composites." *J. Compos. Constr.* 18 (1): 04013025. https://doi.org/10.1061/(ASCE)CC.1943-5614.0000386.

Cao, Y-G, C. Hou, M-Y Liu, and C. Jiang. 2021. "Effects of predamage and load cyclic on compression behavior of fiber reinforced polymer-confined concrete." *Struct. Concr.* 22 (3): 1784–1799. https://doi.org/10.1002/suco.202000568.

Dai, J. G., L. Lam, and T. Ueda. 2012. "Seismic retrofit of square RC columns with polyethylene terephthalate (PET) fibre reinforced polymer composites." *Constr. Build. Mater.* 27 (1): 206–217. https://doi.org/10.1016/j.conbuildmat.2011.07.058.

De Lorenzis, L., and R. Tepfers. 2003. "Comparative study of models on confinement of concrete cylinders with fiber-reinforced polymer composites." *J. Compos. Constr.* 7 (3): 219–237. https://doi.org/10.1061/(ASCE)1090-0268(2003)7:3(219).

Demir, C., K. Darilmaz, and A. Ilki. 2015. "Cyclic stress–strain relationships of FRP confined concrete members." *Arabian J. Sci. Eng.* 40 (2): 363–379. https://doi.org/10.1007/s13369-014-1517-5.

Djafar-Henni, I., and A. Kassoul. 2018. "Stress–strain model of confined concrete with Aramid FRP wraps." *Constr. Build. Mater.* 186: 1016–1030. https://doi.org/10.1016/j.conbuildmat.2018.08.013.

Fallah Pour, A., G. D. Nguyen, T. Vincent, and T. Ozbakkaloglu. 2020. "Investigation of the compressive behavior and failure modes of unconfined and FRP-confined concrete using digital image correlation." *Compos. Struct.* 252: 112642. https://doi.org/10.1016/j.compstruct.2020.112642.

Guo, Y. C., Y. Y. Ye, Guan-Lin, J. F. Lv, Y. L. Bai, and J. J. Zeng. 2020. "Effective usage of high strength steel tubes: Axial compressive behavior of hybrid FRP–concrete–steel solid columns." *Thin-Walled Struct.* 154: 106796. https://doi.org/10.1016/j.tws.2020.106796.

Han, Q., W. Yuan, Y. Bai, and X. Du. 2020. "Compressive behavior of large rupture strain (LRS) FRP-confined square concrete columns: experimental study and model evaluation." *Mater. Struct.* 53 (4): 53–99.

Huang, L., S. S. Zhang, T. Yu, and Z. Y. Wang. 2018. "Compressive behaviour of large rupture strain FRP-confined concrete-encased steel columns." *Constr. Build. Mater.* 183: 513–522. https://doi.org/10.1016/j.conbuildmat.2018.06.074.

Ilki, A., and N. Kumbasar. 2003. "Compressive behaviour of carbon fibre composite jacketed concrete with circular and non-circular cross-sections." *J. Earthquake Eng.* 7 (3): 381–406.

Ilki, A., O. Peker, E. Karamuk, C. Demir, and N. Kumbasar. 2008. "FRP retrofit of low and medium strength circular and rectangular reinforced concrete columns." *J. Mater. Civ. Eng.* 20 (2): 169–188. https://doi.org/10.1061/(ASCE)0899-1561(2008)20:2(169).

Ispir, M. 2015. "Monotonic and cyclic compression tests on concrete confined with PET-FRP." *J. Compos. Constr.* 19 (1): 04014034. https://doi.org/10.1061/(ASCE)CC.1943-5614.0000490.

Ispir, M., K. D. Dalgic, and A. Ilki. 2018. "Hybrid confinement of concrete through use of low and high rupture strain FRP." Composites, Part B 153: 243–255. https://doi.org/10.1016/j.compositesb.2018.07.026.

Downloaded from ascelibrary.org by IZMIR YUKSEK TEKNOLOJI ENSTITUSU on 05/23/22. Copyright ASCE. For personal use only; all rights reserved.

Lam, L., and J. G. Teng. 2003. "Design-oriented stress–strain model for FRP-confined concrete." *Constr. Build. Mater.* 17 (6–7): 471–489. https://doi.org/10.1016/S0950-0618(03)00045-X.
Lam, L., and J. G. Teng. 2004. "Ultimate condition of fiber reinforced polymer-confined concrete." *J. Compos. Constr.* 8 (6): 539–548. https://doi.org/10.1061/(ASCE)1090-0268(2004)8:6(539).
Lam, L., and J. G. Teng. 2009. "Stress–strain model for FRP-confined concrete under cyclic axial compression." *Eng. Struct.* 31 (2): 308–321. https://doi.org/10.1016/j.engstruct.2008.08.014.
Lam, L., J. G. Teng, C. H. Cheung, and Y. Xiao. 2006. "FRP-confined concrete under axial cyclic compression." *Cem. Concr. Compos.* 28 (10): 949–958. https://doi.org/10.1016/j.cemconcomp.2006.07.007.
Li, P., and Y. F. Wu. 2015. "Stress–strain model of FRP confined concrete under cyclic loading." *Compos. Struct.* 134: 60–71. https://doi.org/10.1016/j.compstruct.2015.08.056.
Li, P., Y. F. Wu, and R. Gravina. 2016. "Cyclic response of FRP-confined concrete with post-peak strain softening behavior." *Constr. Build. Mater.* 123: 814–828. https://doi.org/10.1016/j.conbuildmat.2016.07.065.
Lim, J. C., and T. Ozbakkaloglu. 2015. "Lateral strain-to-axial strain relationship of confined concrete." *J. Struct. Eng.* 141 (5): 04014141. https://doi.org/10.1061/(ASCE)ST.1943-541X.0001094.
Lin, G., J. J. Zeng, J. G. Teng, and L. J. Li. 2020. "Behavior of large-scale FRP-confined rectangular RC columns under eccentric compression." *Eng. Struct.* 216: 110759. https://doi.org/10.1016/j.engstruct.2020.110759.
Maeda Kosen. 2002. "Concrete reinforcement Catalogue." Standardization News. Accessed March 14, 2021. https://eng.maedakosen.jp/content/download/9982/97359/file/アンカーメンテ総合カタログ(English) C.2002.00.0101(日C.1910.20.0102.pdf).
Matthys, S., H. Toutanji, and L. Taerwe. 2006. "Stress–strain behavior of large-scale circular columns confined with FRP composites." *J. Struct. Eng.* 132 (1): 123–133. https://doi.org/10.1061/(ASCE)0733-9445(2006)132:1(123).
Nain, M., M. M. Abdulazeez, and M. A. ElGawady. 2020. "Behavior of high strength concrete—filled hybrid large—small rupture strains FRP tubes." *Eng. Struct.* 209: 110264. https://doi.org/10.1016/j.engstruct.2020.110264.
Pessiki, S., K. A. Harries, J. T. Kestner, R. Sause, and J. M. Ricles. 2001. "Axial behavior of reinforced concrete columns confined with FRP jackets." *J. Compos. Constr.* 5 (4): 237–245. https://doi.org/10.1061/(ASCE)1090-0268(2001)5:4(237).
Realfonzo, R., and A. Napoli. 2011. "Concrete confined by FRP systems: Confinement efficiency and design strength models." *Composites, Part B* 42 (4): 736–755. https://doi.org/10.1016/j.compositesb.2011.01.028.
Ribeiro, F., J. Sena-Cruz, F. G. Branco, and E. Júlio. 2018. "Hybrid FRP jacketing for enhanced confinement of circular concrete columns in compression." *Constr. Build. Mater.* 184: 681–704. https://doi.org/10.1016/j.conbuildmat.2018.06.229.
Rousakis, T. C., and A. I. Karabinis. 2008. "Substandard reinforced concrete members subjected to compression: FRP confining effects." *Mater. Struct./Mater. Constr.* 41 (9): 1595–1611. https://doi.org/10.1617/s11527-008-9351-4.
Saleem, S., Q. Hussain, and A. Pimanmas. 2017. "Compressive behavior of PET FRP–confined circular, square, and rectangular concrete columns." *J. Compos. Constr.* 21 (3): 04016097. https://doi.org/10.1061/(ASCE)CC.1943-5614.0000754.
Saleem, S., A. Pimanmas, M. I. Qureshi, and W. Rattanapitikon. 2021. "Axial behavior of PET FRP-confined reinforced concrete." *J. Compos. Constr.* 25 (1): 04020079. https://doi.org/10.1061/(ASCE)CC.1943-5614.0001092.
Teng, J. G., and L. Lam. 2004. "Behavior and modeling of fiber reinforced polymer-confined concrete." *J. Struct. Eng.* 130 (11): 1713–1723. https://doi.org/10.1061/(ASCE)0733-9445(2004)130:11(1713).
TSE (Turkish Standards Institution). 2003. *Testing hardened concrete—Part 3: Compressive strength of test specimens*. TS EN 12390-3. Ankara, Turkey: TSE.
Wu, Y.-F., and Y.-W. Zhou. 2010. "Unified strength model based on Hoek-Brown failure criterion for circular and square concrete columns confined by FRP." *J. Compos. Constr.* 14 (2): 175–184. https://doi.org/10.1061/(ASCE)CC.1943-5614.0000062.
Ye, Y. Y., S. D. Liang, P. Feng, and J. J. Zeng. 2021. "Recyclable LRS FRP composites for engineering structures: Current status and future opportunities." *Composites, Part B* 122: 108689. https://doi.org/10.1016/j.compositesb.2021.108689.
Yönlü, T., and L. P. Kumaş. n.d. "MBRACE® FIBRE.pdf—Google Drive." Accessed March 29, 2021. https://drive.google.com/file/d/1Ky-iuAHS-xHifqJZJhixQoZHPmF5Fha0/view.
Yu, T., B. Zhang, and J. G. Teng. 2015. "Unified cyclic stress–strain model for normal and high strength concrete confined with FRP." *Eng. Struct.* 102: 189–201. https://doi.org/10.1016/j.engstruct.2015.08.014.
Yu, T., S. Zhang, L. Huang, and C. Chan. 2017. "Compressive behavior of hybrid double-skin tubular columns with a large rupture strain FRP tube." *Compos. Struct.* 171: 10–18. https://doi.org/10.1016/j.compstruct.2017.03.013.
Zeng, J. J., Y. Y. Ye, W. Y. Gao, S. T. Smith, and Y. C. Guo. 2020. "Stress–strain behavior of polyethylene terephthalate fiber-reinforced polymer-confined normal-, high- and ultra high-strength concrete." *J. Build. Eng.* 30: 101243. https://doi.org/10.1016/j.jobe.2020.101243.
Zhang, D., Y. Zhao, W. Jin, T. Ueda, and H. Nakai. 2017. "Shear strengthening of corroded reinforced concrete columns using pet fiber based composites." *Eng. Struct.* 153: 757–765. https://doi.org/10.1016/j.engstruct.2017.09.030.

Downloaded from ascelibrary.org by IZMIR YUKSEK TEKNOLOJI ENSTITUSU on 05/23/22. Copyright ASCE. For personal use only; all rights reserved.